Multiple-Energy X-Ray Holography: Atomic Images of Hematite (Fe_2O_3)

T. Gog,[1,2] P. M. Len,[3] G. Materlik,[2] D. Bahr,[2] C. S. Fadley,[3,4] and C. Sanchez-Hanke[2]
[1]*Oak Ridge National Laboratory at the National Synchrotron Light Source, Brookhaven National Laboratory, Upton, New York 11973*
[2]*Hamburger Synchrotronstrahlungslabor (HASYLAB) at Deutsches Elektronen-Synchrotron (DESY), 22603 Hamburg, Germany*
[3]*Department of Physics, University of California at Davis, Davis, California 95616*
[4]*Materials Science Division, Lawrence Berkeley National Laboratory, Berkeley, California 94720*
(Received 20 December 1995)

Multiple-energy x-ray holography (MEXH) is employed to image the local atomic environment of Fe atoms in hematite. MEXH utilizes synchrotron radiation to generate an interference field within the sample, and then determines the strength of this near field at specific atomic sites from the integrated fluorescence yield. Scanning an extended volume of reciprocal space, the local atomic structure in Fe_2O_3 is reconstructed by Fourier transformation from the hologram. Image aberrations known to distort single-energy holograms are effectively suppressed by summing data for several incident energies. [S0031-9007(96)00036-1]

PACS numbers: 61.10.–i, 07.85.–m, 42.40.–i, 61.14.–x

The quest for direct three-dimensional images of atomic structures led Gabor [1] to the discovery of holography in 1948, although atomic resolution was not quite achieved in his time. In recent years it has been pointed out that interference patterns generated by radiation from atomic sources inside a solid, e.g., photoelectrons, Auger electrons, or x rays, can be thought of as a holographic record and that meaningful real-space images can be reconstructed from them [2]. Holographic imaging algorithms for both single- and multiple-energy measurements were put forth [3–5], and, as far as electron emission is concerned, these ideas have been verified experimentally [6–17]. Electron emission holography thus shows considerable promise as a new surface structure probe. Most work in this field has been concerned with photoelectron holography, where the virtue of multiple-energy measurements as a straightforward way to avoid image aberrations is well established [6–13]; however, important contributions also have come from Auger electron holography [14], backscattered Kikuchi holography [15], and diffuse low energy electron and positron diffraction holography [16,17].

For x rays, these holographic ideas are equally if not more attractive. The isotropic nature of the reference and scattering wave fronts, the absence of strong multiple scattering and the longer mean free path make x rays a versatile probe for bulk, surface, and interface investigations. Various possibilities have been explored theoretically and by computer simulation in great detail [18,19]. In fact, experimental atomic images have recently been obtained from a *single-energy* x-ray fluorescence holography (XFH) data set, collected from a $SrTiO_3$ sample [20].

This present work goes beyond XFH, demonstrating a new method that realizes the full potential of *multiple-energy* x-ray holography (MEXH). It can be viewed as a time reversal of the more conventional XFH, utilizing the optical reciprocity theorem in the sense that the positions of radiation source and detector are interchanged and all optical beam paths are reversed. Exploiting this reversal was inspired by an earlier experiment in which x-ray standing waves (XSW) and Kossel lines were found to be intrinsically equivalent, but with XSW yielding superior results over Kossel lines for various practical reasons [21]. XSW and Kossel lines can be considered to be strong diffraction contributions in respective scattering series for which the holographic signal in reversed and conventional geometry is the next weaker single-scattering term. Hence, the same characteristic advantages applying to XSW must apply to MEXH also and it is these advantages that enabled recording an x-ray hologram and reconstructing its holographic image corresponding to the immediate vicinity of Fe atoms in a hematite crystal.

In XFH, depicted in Fig. 1(a), fluorescence from atoms inside the sample is excited by some suitable ionizing radiation, which can be x rays as well as electron or ion beams. Fluorescence from a particular target atom "*A*," approaching a detector located at a large distance from the sample on a direct path, constitutes the holographic reference beam, with energy E_F and wave vector $\vec{k}$. In other directions, fluorescence is scattered by neighboring atoms at positions $\vec{r}_j$. Part of this singly scattered fluorescence, the holographic object beam, will travel directly towards the detector and interfere with the reference beam. By moving the detector on a far-field sphere around the sample, the resulting holographic pattern of intensity $I(\vec{k})$ can be recorded, normalized, and transformed into a real-space reconstructed holographic image $U(\vec{r})$.

With MEXH, shown in Fig. 1(b), the source of radiation and the detector are interchanged. The detector used in XFH is now replaced by a point source of x rays, producing a plane wave with energy E_γ and wave vector $\vec{k}$ at the sample. The target atom *A*, which formerly served as a source of radiation, becomes a detector now, indicating the electric field strength at its core through the total amount of fluorescence it emits in all directions. Thus

 0031-9007/96/76(17)/3132(4)$10.00

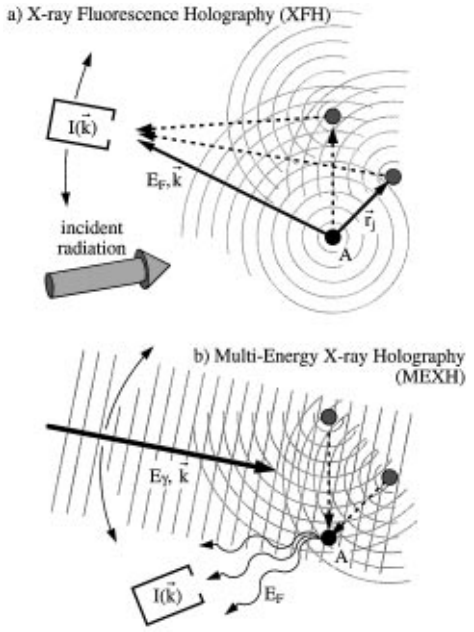

FIG. 1. (a) XFH: externally excited fluorescence from a target atoms *A*, serving as a holographic reference beam, directly approaches a detector located at a large distance from the sample. Fluorescence scattered from neighboring atoms, traveling towards the detector and constituting the object beams, interferes with the reference. Moving the detector around the sample, an intensity pattern $I(\vec{k})$ is recorded which is Fourier transformed to yield an atomic resolution hologram. (b) MEXH: incident monochromatic radiation from a distant point source propagates directly towards a target atom *A*, forming a holographic reference beam. Scattered radiation, serving as the object beam, overlaps and interferes with the reference at *A*. Scanning the wave vector both in direction and magnitude results in an intensity pattern $I(\vec{k})$ at *A*, which is measured by collecting fluorescence emitted from *A* in all directions.

the incident wave front serves as the holographic reference beam, whereas the portion scattered at neighboring atoms, then traveling towards atom *A*, comprises the object beam. Reference and object beams interfere with each other, modulating the electric field at *A*. By scanning the wave vector in direction and magnitude, an intensity pattern $I(\vec{k})$ is generated, which again can be normalized and Fourier transformed to yield an atomic holographic image $U(\vec{r})$.

In summary, the main difference between XFH and MEXH is that XFH utilizes monoenergetic fluorescence from internal atomic sources to generate a holographic scattering field, which is detected in the far field. With MEXH, a tunable incident x-ray beam generates the scattering field; the detector is located in the near field. Fluorescence in the latter case is used as a secondary indicator only; it does not play a role in the generation of the primary scattering field.

By virtue of the optical reciprocity theorem, the two holography schemes described above should in principle be equivalent; however, some practical aspect of MEXH make it superior over XFH. First, with MEXH a monochromatic incident beam is employed, which will not contribute to the signal background at the fluorescence energy as a broadband incident beam can. Second, the linearly polarized character of the incident beam when using synchrotron radiation favors scattering in the plane formed by the beam and the direction perpendicular to its polarization, thereby enhancing the image of atoms in this plane. The information contents of the x-ray hologram in MEXH can be selectively varied and does not require as fine a sampling of reciprocal space as would be the case otherwise. Fluorescence from atomic sources is always unpolarized and does not offer this additional degree of freedom introduced by polarization. Third and most important, the ability to tune the monochromatic incident energy enables sampling a large volume in reciprocal space by varying both the magnitude and direction of $\vec{k}$, thereby avoiding image aberrations which can quite drastically distort holographic images extracted from single-energy data, as discussed previously [18,19]. A proper summation of data collected at different energies will suppress holographic twin images, multiple scattering [4], and accidental image cancellations [19] very effectively, thus reducing the artifacts that plague measurements utilizing only a singe fixed fluorescence energy. It is imagined that the field of application of MEXH will eventually encompass the imaging of solid state surfaces, buried interfaces, which are mostly inaccessible to electron techniques, defect sites in bulk crystals, and other structures involving very diluted constituents, such as nanocrystals or atomic clusters.

To study the feasibility of x-ray holography for atomic resolution imaging, initial measurements were conducted at the Hamburger Synchrotronstrahlungslabor HASYLAB. A set of three-dimensional MEXH data, sufficiently large for reconstruction of a holographic image was later collected at the Oak Ridge National Laboratory beam line X-14A at the National Synchrotron Light Source of Brookhaven National Laboratory. The experimental setup is shown schematically in Fig. 2. A focused, monochromatic x-ray beam is incident on the sample. The sample is mounted on a six-circle diffractometer permitting the required scan motions for holographic recording, namely, a variable inclination Θ of the sample surface with respect to the incident beam and a rotation Φ around the surface normal. Fluorescence emitted from the sample is collected by a cylindrical graphite analyzer with succeeding proportional counter. The angular acceptance of the analyzer was approximately 14° in the direction of the curvature and 0.5° along the straight width. While covering only a small portion of the entire half sphere above the sample this acceptance is large enough to provide averaging of the fluorescence field, thus suppressing local structure such as Kossel lines.

The sample was a natural slab of hematite (Fe_2O_3) with a surface normal parallel to the (001) direction and a mosaic spread of less than 0.01°. The crystal structure of hematite

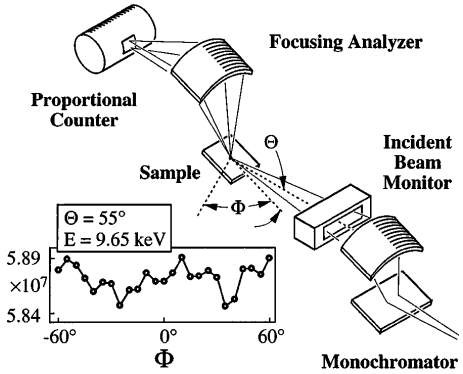

FIG. 2. Experimental configuration for MEXH measurements at beam line X-14. Monochromatic synchrotron radiation is incident on the sample, which is scanned in terms of the inclination angle Θ and azimuthal angle Φ. Fe $K\alpha$ fluorescence is collected by a curved graphite analyzer and proportional counter. A typical Φ scan at $E = 9.65$ keV and $\Theta = 55°$, after correcting for detector dead time, is shown in the inset. The signal modulation is approximately 0.5% of the total counts, on an otherwise constant background.

can be conveniently described in a hexagonal system with lattice constants $a = 5.038$ Å and $c = 13.772$ Å. Viewed along the $\vec{c}$ axis, it consists of alternating layers of iron and oxygen atoms, where iron layers in themselves are separated into two planes spaced about 0.6 Å apart and two different stacking orders exist. A schematic rendering of such an iron layer is shown in Fig. (a). For the first kind of stacking order black circles denote atoms in an upper plane while gray circles are atoms in an lower plane; for the second kind white circles mean upper plane atoms and black circles constitute the lower plane. Since MEXH cannot distinguish between different iron layers, a superposition of both structures is expected to be present in a holographic reconstruction of these layers.

In the present experiment, fluorescence intensities were measured for three incident energies $E_\gamma = 9.00$, 9.65, and 10.30 keV, corresponding to wave-vector magnitudes of $|\vec{k}| = 4.56$, 4.89, and 5.22 Å^{-1}, respectively. Scans were performed on an angular grid of $(\Delta\Theta \times \Delta\Phi) = (5° \times 5°)$ within ranges of $45° \leq \Theta \leq 85°$ and $-60° \leq \Phi \leq +60°$, yielding sufficient energy ($\Delta|\vec{k}|$) and angular $\vec{k}$-space ($|\Delta\vec{k}|$) resolution to avoid coarse sampling alias artifacts for radii smaller than $R < \pi/\Delta|\vec{k}| = 4.38$ Å around an atomic emitter [22]. Thus it should be possible to image the nearest neighbors of Fe in hematite at distances of 2.91 Å. Fluorescence data from a typical Φ scan, collected at an incident energy of 9.65 keV, a Θ angle of 55°, and after applying a correction for dead time effects of the detector, are shown in the inset of Fig. 2. The modulation of the integrated yield displays an amplitude of the order of 0.5% of the total counts on an otherwise constant background. Because of the threefold symmetry about the crystal's $\vec{c}$ axis, the measured intensities $I(\vec{k})$ could be mapped onto the entire 2π hemisphere above the sample. A normalized hologram $\chi(\vec{k})$ was then obtained

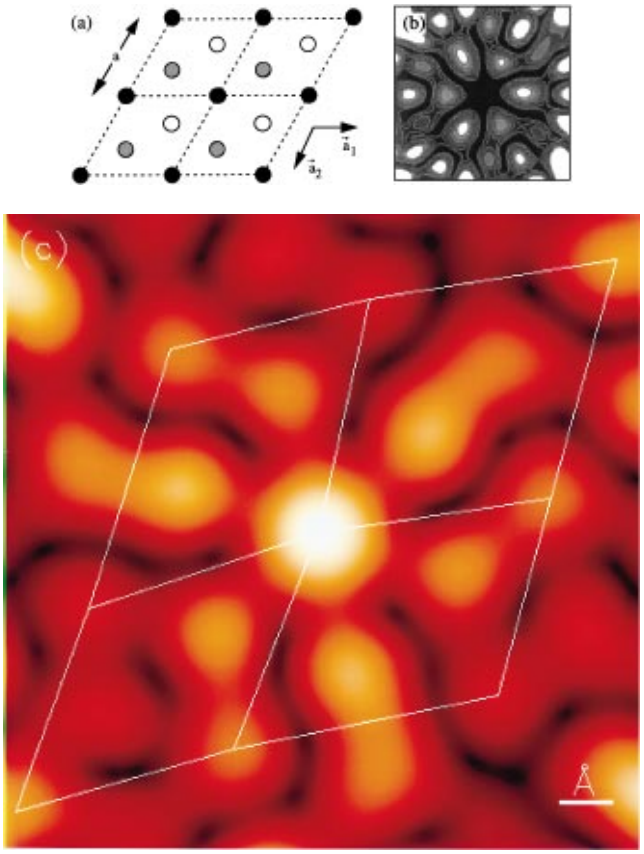

FIG. 3. (a) Structure of a hematite (0,0,1) Fe double layer. Shown are all possible Fe locations for two different stacking orders (refer to text). (b) Image resulting from a theoretical calculation for a hematitelike Fe site. (c) (color) Holographic reconstruction of a (0,0,1) Fe layer of hematite from experimental data. Visible are the six nearest Fe neighbors (three for each kind of stacking order) to the center atom at distances of 2.9 Å. Corner atoms on the hexagonal base grid can be identified up to distances of 8.7 Å.

by subtracting a background fluorescence intensity $I_0(\vec{k})$, which was derived from $I(\vec{k})$ through a Gaussian low-pass convolution [23].

Using algorithms proposed previously for multiple-energy holography [4,5], a real-space atomic image was obtained from $\chi(\vec{k})$ for a basal (0,0,1) plane, passing through an Fe atom. This particular reconstruction, shown in Fig. 3(c), is a superposition of two different Fe layers as described above. Therefore six nearest Fe neighbors of the central emitter (three for each kind of stacking order) appear in the image at distances of 2.9 Å from the center, slightly shifted inwards from their "real" positions due to the small imaginary part of the complex scattering factor of Fe. Corner atoms on the hexagonal grid can be identified unambiguously, even at distances of up to 8.7 Å. Distortions of the grid are due to the angular pattern underlying the data collection which was incommensurate with the crystal symmetry and rather coarse. Images of oxygen atoms were expected to be absent due to a scattering cross section approximately ten times smaller than that of Fe.

To put this holographic image reconstructed from experimental data into perspective, calculations based on clusters of Fe atoms were performed. These clusters were constructed to match the immediate environment of the two Fe sites present in hematite. An image reconstructed from these theoretical data, shown in Fig. (b), agreed well with the experiment.

Besides imaging the (0,0,1) plane, an attempt was made to reconstruct the hematite (1,1,0) plane. Not all of the Fe atoms expected to appear were visible, which is attributed to a loss of image resolution along the $\vec{c}$ axis as a direct consequence of the limited range of energy and solid angle available as well as the nature of the scattering of the polarized incident synchrotron radiation. Images of this plane should become further resolved with extended data scans and a different orientation of the sample with respect to the incident direction of polarization.

While these first MEXH results are very encouraging, several issues have to be addressed before this method can be promoted into the sphere of routine analytical tools. A primary concern is the data acquisition time for a complete x-ray hologram, which was of the order of 150 h in the current experiment and is directly related to the capability of the detector to record fluorescence at high count rates. Recording at $\approx 10^6$ s^{-1} would be desirable, but at the same time it is necessary to disperse energy sufficiently to clearly separate fluorescence from the incident beam. Studies now underway using a faster detector indicate that, for bulk crystals, a reduction of data acquisition time by 1 order of magnitude is readily achievable. To make samples with diluted constituents accessible to this method, however, will require a detector which covers a much larger solid angle than presently available, in combination with higher quantum efficiency and an increase in incident flux.

Nonetheless, the results presented above demonstrate that multiple-energy x-ray holograms are feasible and that this method shows promise of becoming a powerful new tool for directly imaging atomic structures in the bulk or at surfaces and interfaces of solids.

The authors are indebted to K. F. Finkelstein for providing the hematite sample, to R. H. Menk for help with the graphical representations, and to D. Novikov for many fruitful discussions. This research was performed in part at the Oak Ridge National Laboratory beam line X-14 at the National Synchrotron Light Source, Brookhaven National Laboratory, sponsored by the Division of Material Sciences and Division of Chemical Sciences, U.S. Department of Energy and under Contract No. DE-AC05-840R21400 with the Lockheed-Martin Energy Systems, Inc. Research at UC Davis is supported in part by the Office of Naval Research under Contracts No. N00014-90-5-1457 and No. N00014-94-1-0162, by the Director of the Office of Energy Research, Office of Basic Energy Sciences, Material Sciences Division of the U.S. Department of Energy, Contract No. DE-AC03-76SF00098 and by the National Energy Research Supercomputer Center.

[1] D. Gabor, Nature (London) **161**, 777 (1948).
[2] A. Szöke, in *Short Wavelength Coherent Radiation: Generation and Applications*, edited by D. T. Attwood and J. Bokor, AIP Conf. Proc. No. 147 (AIP, New York, 1986).
[3] J. J. Barton, Phys. Rev. Lett. **61**, 1356 (1988).
[4] J. J. Barton, Phys. Rev. Lett. **67**, 3106 (1991).
[5] S. Y. Tong, H. Huang, and C. M. Wei, Phys. Rev. B **46**, 2452 (1992).
[6] S. Thevuthasan, R. X. Ynzunza, E. D. Tober, C. S. Fadley, A. P. Kaduwela, and M. A. Van Hove, Phys. Rev. Lett. **70**, 595 (1993).
[7] L. J. Terminello, J. J. Barton, and D. A. Lapiano-Smith, Phys. Rev. Lett. **70**, 599 (1993).
[8] M. T. Sieger, J. M. Roesler, D.-S. Lin, T. Miller, and T.-C. Chiang, Phys. Rev. Lett. **73**, 3117 (1994).
[9] B. L. Petersen, L. J. Terminello, J. J. Barton, and D. A. Shirley, Chem. Phys. Lett. **220**, 46 (1994).
[10] J. G. Tobin, G. D. Waddill, H. Li, and S. Y. Tong, Phys. Rev. Lett. **70**, 4150 (1993).
[11] H. Wu, G. J. Lapeyre, H. Huang, and S. Y. Tong, Phys. Rev. Lett. **71**, 251 (1993).
[12] B. P. Tonner, Z.-L. Han, G. R. Harp, and D. K. Saldin, Phys. Rev. B **43**, 14 423 (1991).
[13] M. Zharnikov, M. Weinelt, P. Zebisch, M. Stichler, and H.-P. Steinrück, Phys. Rev. Lett. **73**, 3548 (1994).
[14] H. Li, S. Y. Tong, D. Naumovic, A. Stuck, and J. Osterwalder, Phys. Rev. B **47**, 10 036 (1993); D. K. Saldin, G. R. Harp, and X. Chen, Phys. Rev. B **48**, 8234 (1993).
[15] G. R. Harp, D. K. Saldin, and B. P. Tonner, Phys. Rev. Lett. **65**, 1012 (1990); Z.-L. Han, S. Hardcastle, G. R. Harp, H. Li, X.-D. Wang, J. Zhang, and B. P. Tonner, Surf. Sci. **258**, 313 (1991); P. R. Jeng, I. H. Hong, Y. C. Chou, and C. M. Wei, Phys. Rev. B **51**, 13 645 (1995).
[16] D. K. Saldin and P. L. De Andres, Phys. Rev. Lett. **64**, 1270 (1990); M. A. Mendez, C. Glück, J. Guerrero, P. L. De Andres, K. Heinz, D. K. Saldin, and J. B. Pendry, Phys. Rev. B **45**, 9402 (1992); C. M. Wei, S. Y. Tong, H. Wedler, M. A. Mendez, and K. Heinz, Phys. Rev. Lett. **72**, 2434 (1994).
[17] S. Y. Tong, H. Huang, and X. Q. Guo, Phys. Rev. Lett. **69**, 3654 (1992), (and many other references proposing modifications to the basic ideally optical holographic reconstruction algorithm that attempt to correct for the nonideal reference, scattering, and propagation nature of electron wave fronts).
[18] M. Tegze and G. Faigel, Europhys. Lett. **16**, 41 (1991).
[19] P. M. Len, S. Thevuthasan, C. S. Fadley, A. P. Kaduwela, and M. A. Van Hove, Phys. Rev. B **50**, 11 275 (1994).
[20] M. Tegze and G. Faigel (to be published).
[21] T. Gog, D. Bahr, and G. Materlik, Phys. Rev. B **51**, 6761 (1995).
[22] P. M. Len, S. Thevuthasan, A. P. Kaduwela, M. A. Van Hove, and C. S. Fadley (to be published); P. M. Len, F. Zhang, S. Thevuthasan, A. P. Kaduwela, M. A. Van Hove, and C. S. Fadley (to be published).
[23] G. R. Harp, D. K. Saldin, X. Chen, Z.-L. Han, and B. P. Tonner, J. Electron Spectrosc. Relat. Phenom. **70**, 331 (1991).